J. Phys. B: At. Mol. Phys. 17 (1984) 3279–3294. Printed in Great Britain

The elastic scattering of electrons from inert gases: IV. Krypton

W C Fon†‡, K A Berrington and A Hibbert

Department of Applied Mathematics and Theoretical Physics, The Queen's University of Belfast, Belfast BT7 1NN, Northern Ireland

Received 13 February 1984

Abstract. The calculations of Fon *et al* on electrons colliding with helium, neon and argon in which the atomic ground-state wavefunction is coupled with a ^1P pseudo-state to allow for the dipole polarisability are extended to consider the elastic scattering of electrons from krypton. Phaseshifts, differential, integral and momentum transfer cross sections are reported for electron impact energies ranging from 0.1 to 120 eV.

1. Introduction

This paper is the fourth in a series which studies phaseshifts, integral, differential and momentum transfer cross sections of electrons elastically scattered from inert-gas atoms calculated using the R-matrix method. Details of the calculations are to be found in Fon *et al* (1981), Fon and Berrington (1981) and Fon *et al* (1983) (hereafter referred to as I, II and III, respectively), which describe electron scattering from helium, neon and argon, respectively. The method is now extended to krypton.

Early measurements on elastic differential cross sections for Kr were reported by Arnot (1931), Ramsauer and Kollath (1932), Webb (1935) and then followed by the works of Mehr (1967), Schackert (1968), Lewis *et al* (1974) and Heindörff *et al* (1976). Unfortunately these earlier experiments were not absolute and only recently Bromberg (1974), Williams and Crowe (1975), Jansen *et al* (1976) and Srivastava *et al* (1981) reported absolute differential cross sections for Kr (see Bransden and McDowell 1978, Kieffer 1971, for reviews). However, agreement among these absolute measurements is less than satisfactory. Generally, they suffer from two serious drawbacks: (i) the measured energy points are few and hence they are unable to describe the rapidly changing pattern of the differential cross sections as the incident energy moves across the intermediate energy range (especially over the energy range from 20–150 eV); (ii) due to inherent difficulties arising from the experimental set-up, they are limited in angular range especially at small scattering angles ($\theta < 20°$) and large scattering angles ($\theta > 150°$). This second limitation seriously weakens their ability to establish fully the shape of the differential cross section over the whole angular range ($0 \leqslant \theta \leqslant \pi$), as in the case of Kr, one of the dips might well lie beyond 150°. This limitation has another serious consequence. To obtain total (integrated) cross sections, the differential cross

† Present address: International Centre for Theoretical Physics, PO Box 586-34100, Trieste, Italy.
‡ ICTP Associate on research leave from the Department of Mathematics, University of Malaya, Kuala Lumpur, Malaysia.

0022-3700/84/163279+16$02.25 © 1984 The Institute of Physics

sections have to be integrated over the whole solid angle. To do this the experimentalists are forced to employ methods of extrapolation which in some cases are less than sound in principle to obtain differential cross sections at angles which cannot be measured. The contribution from these scattering angles is by no means negligible and is known to affect significantly the overall normalisation of the cross sections. It is therefore desirable that an independent and *ab initio* calculation be performed to complement and guide future experimental work.

A rigorous theoretical treatment of elastic scattering of electrons from inert-gas atoms is considered very complicated (Kemper *et al* 1983). Hence calculations of elastic cross sections for krypton have been considered only in the form of a single-particle potential model (Holtsmark 1930, Berg *et al* 1971, Lewis *et al* 1974, Yau *et al* 1980, Berg 1982). Although they did provide a reasonable fit to the experimental data for lighter rare-gas atoms, they were far from satisfactory in predicting the elastic differential cross sections for krypton especially at electron impact energies less than 100 eV. Attempts have been made to include relativistic effects and spin–orbit interaction (semi-phenomenological optical potential method: McCarthy *et al* (1977); Kemper *et al* (1983); semi-relativistic model: Sin Fai Lam (1982); solution of the Dirac equation: Fink and Yates (1970), Walker (1971)). However, the discrepancy between the theories and the experiments does not seem to have been resolved in the intermediate energy range. The indication is that spin–orbit interaction and other relativistic effects might not be as significant as one has been led to believe. Sin Fai Lam (1982) showed that in the case of elastic scattering of low energy electrons from krypton, these relativistic effects are not significant.

In this paper, the simplicity of the treatment used in I–III is preserved. It is assumed that the spin–orbit interaction and other relativistic effects are not important in the elastic scattering of electrons from neutral krypton. The polarisation, exchange and absorption effects are built in a natural way by coupling the krypton ground state to a ^{1}P pseudo-state. The present paper thus represents an *ab initio* attempt to obtain elastic scattering cross sections of electrons on krypton over a wide range of energies (0.1–120 eV) which, while not expected to be of the highest accuracy, should give a reasonable representation of the essential physical features.

2. *R*-matrix calculation

The *R*-matrix program described by Berrington *et al* (1978) is used to calculate the phaseshifts and *K*-matrix elements. The *R*-matrix radius is taken to be 11 au and the number of continuum orbitals included for each angular momentum is 13. The Kr ground-state wavefunction is coupled with a ^{1}P pesudo-state to allow for the ground-state static dipole polarisability. This requires the solution of a problem with two coupled channels when the total angular momentum $L = 0$, and three coupled channels when $L \geqslant 1$. While the Hartree–Fock (HF) Kr ground-state wavefunction is given by Clementi and Roetti (1974), the ^{1}P pseudo-state is expressed as a linear combination of five configurations, namely:

$$a_1(1s^2 2s^2 2p^6 3s^2 3p^6 3d^{10} 4s 4p^6 \overline{5p}) + a_2(1s^2 2s^2 2p^6 3s^2 3p^6 3d^{10} 4s^2 4p^5 \overline{5s}) + a_3(1s^2 2s^2 2p^6 3s^2 3p^6 3d^{10} 4s^2 4p^5 \overline{5d}) + a_4(1s^2 2s^2 2p^6 3s^2 3p^6 3d^{10} 4s^2 4p^5 \overline{4d}) + a_5(1s^2 2s^2 2p^6 3s^2 3p^6 3d^9 4s^2 4p^6 \overline{4f}) \quad (1)$$

where $a_1 = -0.076\,5070$, $a_2 = 0.522\,7948$, $a_3 = 0.653\,7643$, $a_4 = -0.541\,5066$ and $a_5 = 0.013\,9669$.

The one-electron radial orbitals are expressed in the form

$$P_{nl}(r) = \sum_i C_i r^{P_i} \exp(-\xi_i r). \tag{2}$$

The parameters $\{C_i\}$, $\{P_i\}$ and $\{\xi_i\}$ for 1s, 2s, 2p, 3s, 3p, 3d, 4s and 4p are taken from Clementi and Roetti (1974). The parameters for the other orbitals are given in table 1. Those for $\overline{4d}$ are determined by optimising the ground-state energy including near-degeneracy effects, using the CIV3 program of Hibbert (1975). Those for the pseudo-orbitals $\overline{5s}$, $\overline{5p}$ and $\overline{5d}$ and $\overline{4f}$ are determined by optimising the ground-state static dipole polarisability following Vo Ky Lan *et al* (1976) using the code CIVPOL with a single configuration ground state and a ^{1}P pseudo-state defined by (1). The ground-state energy is $-2752.054\,125$ au while the CI wavefunction for the ^{1}P pseudo-state gives a polarisability equal to 19.7 au. This compares with the experimental value of 16.8 au (Landolt-Börnstein 1950). This represents a 15% deviation from the experimental value which should not unduly affect the accuracy of the present calculations in the intermediate energy range considered here, as was shown by the previous calculations for Ar (see III) in which the calculated dipole polarisability for the Ar ground state deviated from the experimental value by a similar amount.

Table 1. Values of parameters for the pseudo-orbitals.

Orbital	C_i Slater-type coefficients	P_i	ξ_i
$\overline{4d}$	127.212 79	3	6.645 95
	−11.090 22	4	2.750 50
$\overline{4f}$	30.608 32	4	3.474 41
$\overline{5s}$	7.877 78	1	18.503 16
	−125.501 81	2	15.027 35
	99.805 74	3	7.480 20
	−18.602 46	4	3.242 69
	0.154 33	5	1.398 28
$\overline{5p}$	143.938 18	2	15.333 51
	−150.946 31	3	7.004 49
	21.229 28	4	3.270 46
	−0.447 67	5	1.702 28
$\overline{5d}$	38.701 87	3	5.489 03
	−13.259 72	4	3.333 09
	0.169 75	5	1.420 47

The excellent agreement between the calculation of III and experiments for Ar can be explained by the observation on apparent polarisabilities for inert gases reported by Jansen *et al* (1976) and Jansen and de Heer (1976) (see table 2). It is clear that the static dipole polarisabilities for Ne, Ar and Kr are considerably lower than the 'apparent' polarisabilities (Jansen *et al* 1976) over the intermediate energy range. This is because the frequency-dependent polarisability increases from the exact static dipole polarisability at zero energy, reaches a maximum value before or around 100 eV, then

Table 2. Apparent and static polarisabilities for Ne, Ar and Kr (in units of a_0^3) (from Jansen *et al* 1976 and Jansen and de Heer 1976).

E (eV)	Ne	Ar	Kr
100	3.09	14.8	22.4
150	2.88	13.9	19.8
200	2.82	12.2	19.1
300	2.62	10.6	15.6
400	2.48	9.57	13.1
500	2.26	8.44	12.9
750	1.98	7.77	11.9
1000	1.88	7.55	11.6
2000	1.86	7.40	11.4
3000	1.78	7.53	13.4
static	2.69	11.0	16.8

follows a monotonic descent passing the exact value of static dipole polarisability on the way down at around 300 eV. Therefore it is not unreasonable to suggest that the polarisabilities calculated in this paper and in III for Kr and Ar do represent realistic effective polarisabilities for these atoms in the energy range from a few electron volts to 200 eV. At very low energies, the dominant role of the dipole polarisation is challenged by the contribution from higher multipoles, and short-range correlations too are expected to play an important role in the close-range collision. However, encouraged by the success achieved in I to III, the present calculation is extended to energies as low as 0.1 eV.

In the present calculation, only partial waves up to $L = 13$ are calculated directly by the R-matrix program; for $L > 13$, the T-matrix elements converge well (see table 4) to those obtained using the effect-range theory (ERT) of Rosenberg *et al* (1961):

$$\tan \delta_L = \frac{\pi \alpha k^2}{(2L+3)(2L+1)(2L-1)} \tag{3}$$

where α is the calculated dipole polarisability. Hence the T-matrix elements can be obtained as follows

$$T_L = 2\mathrm{i} \tan \delta_L - 2(\tan \delta_L)^2. \tag{4}$$

For energies above 50 eV, a few more partial waves ($L > 13$) are extrapolated to give smooth convergence to the ERT values. The highest partial wave included is $L = 450$ for $E = 120$ eV.

Pseudo-resonances due to the ^{1}P pseudo-threshold at 16.75 eV and to the $(N+1)$ electron correlation terms occur over the energies ranging from 16 to 70 eV. The T-matrix elements for impact energies in this region are extracted by an averaging technique described in a previous paper (Burke *et al* 1981). Notice that above the ^{1}P pseudo-threshold the atom can be excited into the pseudo-state. This makes some allowance for inelasticity effects in the calculations for energies above pseudo-threshold and closed-channel effects upon the elastic channel for energies below pseudo-threshold.

3. Results and discussion

Phaseshifts, integral, elastic differential and momentum transfer cross sections are calculated for the following process.

$$e + Kr(^1S_0) \rightarrow e + Kr(^1S_0)$$

at impact energies ranging from 0.1 to 120 eV. The present calculations are given in tables 3 to 7 and figures 1 to 5, where comparisons with other theoretical calculations and experimental measurements are also made.

3.1. Phaseshifts

In table 3, the present calculated phaseshifts for $L = 0$, 1, 2, 3, 4 are presented and these are compared in figure 1 with the polarised-orbital calculations of Yau *et al* (1980) and those semi-relativistic calculations of Sin Fai Lam (1982). No other phaseshift analysis from experimental measurements has been reported except that of Srivastava *et al* (1981), which exhibits irregular freatures as in the case of Ar.

Table 3. Phaseshifts (in rad) for the elastic scattering of electrons from krypton atoms. The superscript denotes the power of ten by which the number should be multiplied.

E (eV)	k^2(Ryd)	δ_0	δ_1	δ_2	δ_3	δ_4
0.1	0.007 3510	0.1628	0.2074^{-1}	0.4362^{-2}	0.1427^{-2}	0.6599^{-3}
0.2	0.014 7012	0.1464	0.3338^{-1}	0.9031^{-2}	0.2903^{-2}	0.1317^{-2}
0.4	0.029 4016	0.8332^{-1}	0.4348^{-1}	0.1917^{-1}	0.5851^{-2}	0.2629^{-2}
0.6	0.044 1020	0.1727^{-1}	0.4049^{-1}	0.3035^{-1}	0.8887^{-2}	0.3945^{-2}
0.8	0.058 8024	-0.4481^{-1}	0.2918^{-1}	0.4231^{-1}	0.1207^{-1}	0.5276^{-2}
1.0	0.073 5028	−0.1023	0.1259^{-1}	0.5506^{-1}	0.1540^{-1}	0.6638^{-2}
2.0	0.147 0048	−0.3358	−0.1002	0.1246	0.3336^{-1}	0.1423^{-1}
3.0	0.220 5072	−0.5157	−0.2157	0.2053	0.4983^{-1}	0.2306^{-1}
4.0	0.294 0096	−0.6672	−0.3193	0.3047	0.6279^{-1}	0.3183^{-1}
5.0	0.367 5120	−0.7998	−0.4116	0.4228	0.7373^{-1}	0.3934^{-1}
6.0	0.441 0144	−0.9176	−0.4950	0.5516	0.8471^{-1}	0.4548^{-1}
7.0	0.514 5168	-0.1023^{1}	−0.5710	0.6813	0.9668^{-1}	0.5091^{-1}
8.0	0.588 0192	-0.1119^{1}	−0.6407	0.8042	0.1096	0.5639^{-1}
9.0	0.661 5216	-0.1207^{1}	−0.7047	0.9155	0.1231	0.6234^{-1}
10.0	0.735 0240	-0.1288^{1}	−0.7635	0.1013^{1}	0.1371	0.6881^{-1}
11.0	0.808 5264	-0.1364^{1}	−0.8176	0.1096^{1}	0.1518	0.7562^{-1}
12.0	0.882 0288	-0.1435^{1}	−0.8674	0.1165^{1}	0.1678	0.8254^{-1}
13.0	0.955 5312	-0.1502^{1}	−0.9132	0.1222^{1}	0.1855	0.8950^{-1}
14.0	1.029 0366	-0.1565^{1}	−0.9552	0.1271^{1}	0.2055	0.9653^{-1}
15.0	1.102 5360	-0.1626^{1}	−0.9928	0.1312^{1}	0.2285	0.1037

In figure 1(*a*), the present *R*-matrix calculations of S- and P-wave phaseshifts are seen to be in good agreement with those of Sin Fai Lam (1982) and those of O'Connell and Lane (1983) (not shown) but are considerably lower than those of Yau *et al* (1980). Figures 1(*b*) and (*c*) compare *R*-matrix D and F phaseshifts with those of Sin Fai Lam (1982) and Yau *et al* (1980). Again as in the case of Ar, the

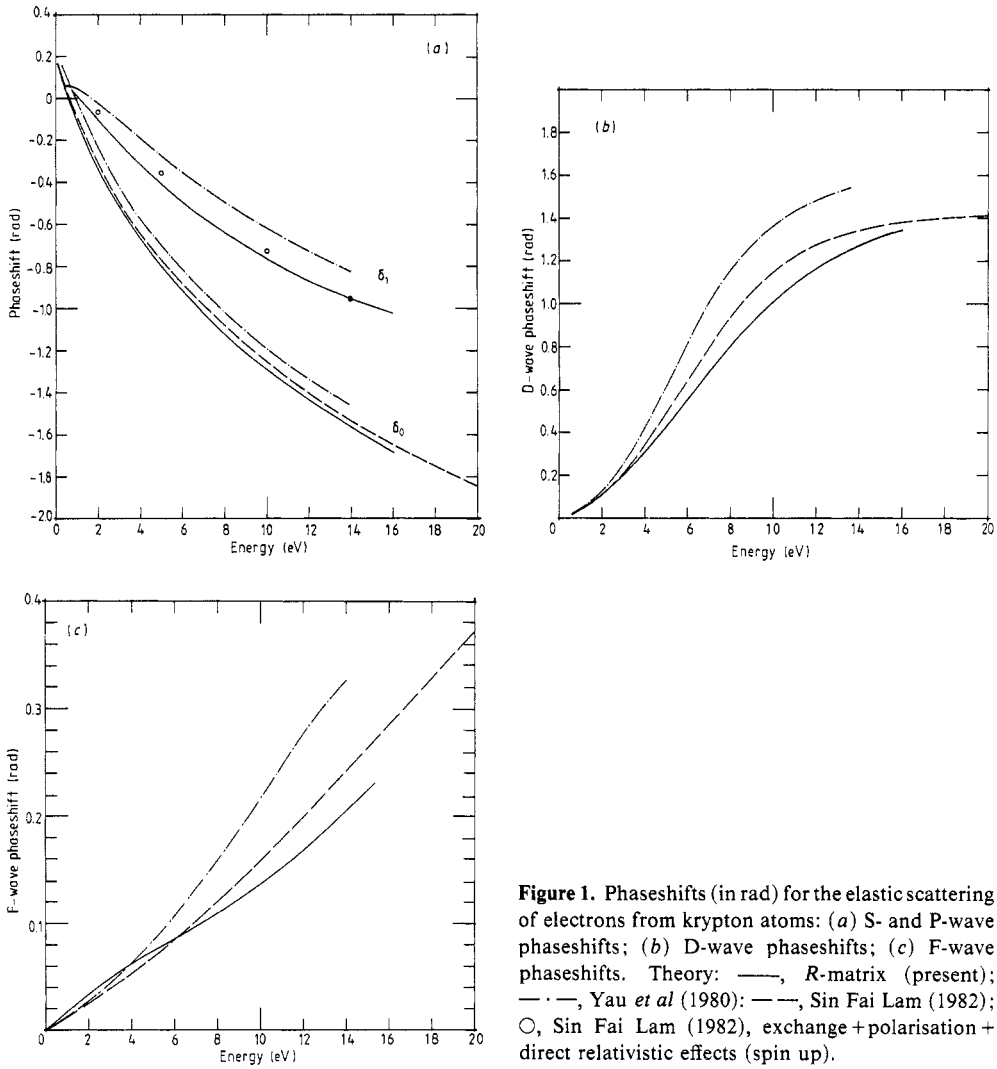

Figure 1. Phaseshifts (in rad) for the elastic scattering of electrons from krypton atoms: (*a*) S- and P-wave phaseshifts; (*b*) D-wave phaseshifts; (*c*) F-wave phaseshifts. Theory: ——, *R*-matrix (present); — · —, Yau *et al* (1980): — —, Sin Fai Lam (1982); ○, Sin Fai Lam (1982), exchange + polarisation + direct relativistic effects (spin up).

polarised-orbital calculations of Yau *et al* (1980) lie substantially higher than the *R*-matrix phaseshifts. The agreement between *R*-matrix calculations and those of Sin Fai Lam (1982) for D and F waves is not as good as in the case for S and P waves. The most recent calculations of O'Connell and Lane (1983) are in best agreement with the present calculations. However, it is important to note that any agreement between the present calculations and those of Sin Fai Lam (1982) should be viewed with caution, as Sin Fai Lam used a procedure in which the polarisation potential (first obtained by the Pople–Schofield method) was renormalised to give the experimental value of the static dipole polarisability in the limit of $r \to \infty$. As pointed out in § 2, the effective polarisability for non-zero energies is most likely considerably larger than the experimental static dipole polarisability. It is not clear to what extent the renormalisation procedure used by Sin Fai Lam (1982) would affect his result, if the dipole polarisability were not taken to be the static dipole polarisability.

In table 4, the present R-matrix calculations for the higher partial-wave phaseshifts are compared with those obtained using the ERT formula of Rosenberg *et al* (see equation (3)). The indication is that the present R-matrix phaseshifts converge rapidly towards the ERT values as L increases.

Table 4. Comparison of phaseshifts with ERT. A, ERT phaseshifts (with the calculated dipole polarisability $\alpha = 19.6967$ au). B, R matrix (present calculation).

	$E = 1$ eV		$E = 3$ eV		$E = 5$ eV		$E = 10$ eV	
δ_L(rad)	A	B	A	B	A	B	A	B
3	0.014 44	0.015 40	0.043 29	0.049 83	0.072 07	0.073 73	0.143 40	0.130 69
4	0.006 56	0.006 64	0.019 69	0.023 06	0.032 80	0.039 34	0.065 54	0.063 35
5	0.003 53	0.003 53	0.010 60	0.011 41	0.017 67	0.021 42	0.035 33	0.034 22
6	0.002 10	0.002 11	0.006 36	0.006 46	0.010 60	0.011 87	0.021 20	0.020 83
7	0.001 37	0.001 37	0.004 12	0.004 11	0.006 86	0.007 12	0.013 72	0.013 50
8	—	—	0.002 82	0.002 81	0.004 69	0.004 71	0.009 39	0.009 24

3.2. Integral elastic and momentum transfer cross sections

The present calculations of integral elastic and momentum transfer cross sections are summarised in tables 5–6 and compared with other theoretical calculations and experimental measurements in table 5 and in figures 2–3.

Figure 2 shows that there is satisfactory agreement between the present calculations for the elastic integral cross sections and those measured by Ramsauer and Kollath (1929) at very low energies. The Ramsauer–Townsend minimum is clearly reproduced by the present calculation at 0.7 eV, despite the lack of accuracy in the calculated cross sections at this low energy due to the inadequate representation of correlation and

Table 5. Integral elastic cross section (in units of a_0^2) for electron–krypton scattering at intermediate energies. A, R matrix (present); B, semi-empirical (de Heer *et al* 1979); C, Williams and Crowe (1975); D, Jansen and de Heer (1976); E, Srivastava *et al* (1981); F, relativistic + static + exchange (Walker 1971, 1974); G, relativistic + static + exchange + polarisation (Walker 1971, 1974); H, semi-relativistic (static + exchange + polarisation) (Sin Fai Lam 1982).

E(ev)	A	B	C	D	E	F	G	H
20	77.66	71.80	71.80		57.86	68.94	82.05	81.54
30	56.21	49.08	49.08		37.14	49.75	63.47	62.96
40	43.17	37.79	37.79			39.50	52.43	
50	35.61	32.46	32.46		31.79	33.60	45.00	
60	30.63						39.50	
70	28.26							
80	25.93							
90	23.97							
100	23.00	22.10	27.09	22.91	14.29	21.42	27.52	
110	22.34							
120	21.82							
150	—	15.68		16.26			20.85	

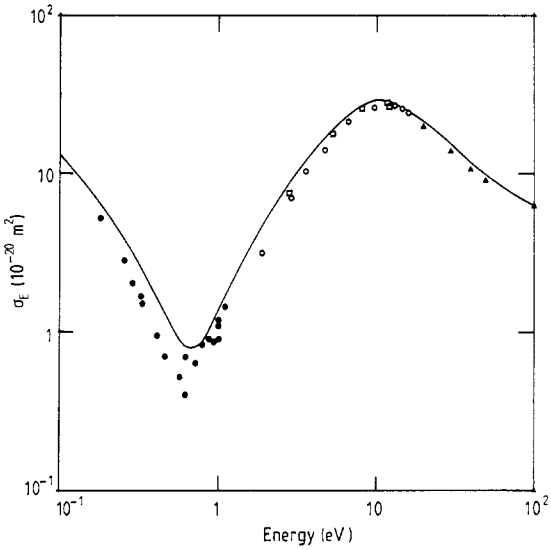

Figure 2. Integral elastic cross section (10^{-20} m^2). Experiment: ●, Ramsauer and Kollath (1929); □, Ramsauer (1923); ○, Dababneh *et al* (1980); △, de Heer *et al* (1979). Theory: ——, *R* matrix (present).

polarisability effects. From a few eV to energies below the first excitation threshold, the present calculations are also in good agreement with the experiments of Ramsauer (1923) and Dababneh *et al* (1980). In particular the cross section maximum at around 10 eV is reproduced by the present calculation while the calculation of Yau *et al* (1980) and Sin Fai Lam (1982) overestimate the cross section over the energy range from 5–15 eV. This is mainly due to large values of their D- and F-wave phaseshifts. At energies above 20 eV, there is an excellent agreement between the present calculations and the semi-empirical cross sections of de Heer *et al* (1979).

Table 5 shows there is good agreement between the present calculations and those of Walker (1971, relativistic + static + exchange), which in turn seems to be in excellent agreement with experiment (de Heer *et al* 1979). However, when polarisation is included, the calculations of Walker tend to diverge from the experiments. The expected consistence of Walker's model is not maintained. The most recent measurements of Srivastava *et al* (1981) seem rather low.

The present calculations of momentum transfer cross section are given in table 6 and compared with other theoretical calculations and the experiments of Frost and Phelps (1964) in figure 3. The agreement between the theoretical calculations and the measurements of Frost and Phelps (1964) is less satisfactory. In general, the theories predict a sharp minimum around the position of the Ramsauer minimum while Frost and Phelps (1964) observed a broad minimum. Below the minimum, the calculations of Yau *et al* (1980) lie considerably higher than the experiments while the present *R*-matrix calculations agree reasonably well with the experiment, though, in view of possible inaccuracies in the present calculation at these low energies, this agreement may be spurious. At higher energies, the theoretical calculations are consistent with one another while differing substantially from the experiments. For all the energies considered by Sin Fai Lam (1982), the present *R*-matrix calculations are in good accord with the calculations of Sin Fai Lam (1982) (not shown in figure 3 for the sake of clarity).

Table 6. Integral elastic and momentum transfer cross sections (present results) at low energies.

E(eV)	$Q_E(10^{-20}\,m^2)$	$Q_{MT}(10^{-20}\,m^2)$	E(eV)	$Q_E(10^{-20}\,m^2)$	$Q_{MT}(10^{-20}\,m^2)$
0.10	12.872	9.586	4.00	13.999	11.683
0.20	5.934	3.315	5.00	18.157	15.307
0.30	3.100	1.182	6.00	22.040	18.222
0.40	1.760	0.399	7.00	25.270	19.972
0.50	1.115	0.164	8.00	27.592	20.495
0.60	0.845	0.179	9.00	28.963	20.042
0.70	0.795	0.317	10.00	29.505	18.968
0.80	0.894	0.525	11.00	29.200	17.436
0.90	1.091	0.772	12.00	28.928	16.146
1.00	1.354	1.042	13.00	28.198	14.755
1.50	3.228	2.602	14.00	27.360	13.500
2.00	5.414	4.315	15.00	26.499	12.359
3.00	9.779	7.927	16.00	25.548	11.392

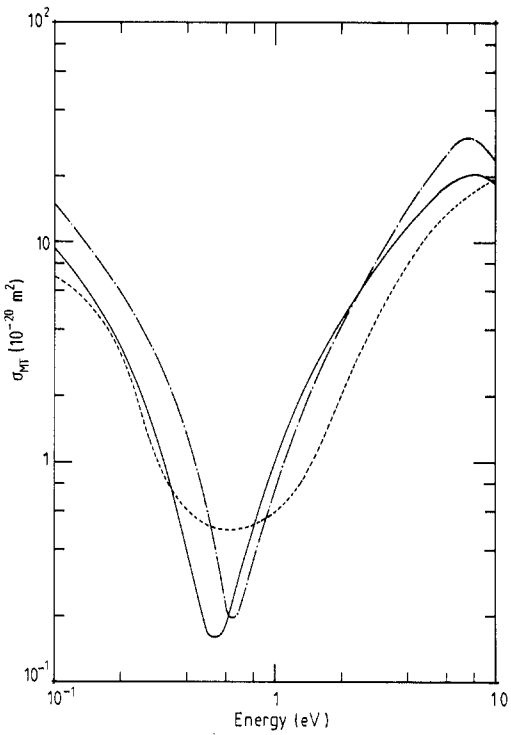

Figure 3. Momentum transfer cross section ($10^{-20}\,m^2$) at low energies. Experiment: · · · · · · · , Frost and Phelps (1964); Theory: ——, R matrix (present); — · —, Yau *et al* (1980).

3.3. Differential cross sections

The present calculation of the elastic differential cross sections is summarised in table 7. Comparison with other calculations and experiments is made in figures 4–5.

Table 7. Differential cross sections for elastic electron–krypton scattering (in units of 10^{-19} cm^2 sr^{-1}) and momentum transfer cross sections σ_{MT} (in units of 10^{-20} m^2). The superscript denotes the power of ten by which the number should be multiplied. The angles θ^1, θ^2, θ^3 correspond to the approximated angular positions of the minima.

	E(eV)				
θ (deg)	1	3	5	10	15
0	1.344^3	2.192^3	6.746^3	2.189^4	2.629^4
5	9.958^2	1.512^3	5.340^3	1.905^4	2.260^4
10	6.729^2	9.521^2	4.046^3	1.615^4	1.899^4
15	4.258^2	5.954^2	3.065^3		
20	2.457^2	4.117^2	2.369^3	1.130^4	1.320^4
25	1.227^2	3.725^2	1.926^3		
30	4.712^1	4.457^2	1.696^3	7.550^3	8.694^3
35	9.633	5.978^2	1.629^3		
40	1.346	7.948^2	1.673^3	4.704^3	5.110^3
45	1.403^1	1.005^3	1.779^3		
50	4.028^1	1.202^3	1.906^3	2.721^3	2.510^3
55					
60	1.086^2	1.472^3	2.104^3	1.622^3	1.005^3
65					6.166^2
70	1.672^2	1.513^3	2.107^3	1.200^3	4.105^2
75					3.360^2
80	1.951^2	1.326^3	1.854^3	1.053^3	3.454^2
85					3.973^2
90	1.878^2	9.816^2	1.369^3	8.591^2	4.566^2
95					4.963^2
100	1.531^2	5.843^2	7.677^2	5.315^2	5.007^2
105			4.838^2	3.489^2	4.681^2
110	1.051^2	2.457^2	2.484^2	1.898^2	4.111^2
115		1.281^2	8.852^1	9.122^1	3.538^2
120	5.823^1	5.668^1	2.728^1	9.266^1	3.243^2
125		3.588^1	8.085^1	2.292^2	3.495^2
130	2.332^1	6.680^1	2.565^2	5.243^2	4.489^2
135	1.203^1	1.467^2	5.511^2	9.843^2	6.312^2
140	4.945	2.691^2	9.513^2	1.598^3	8.970^2
145	1.677	4.243^2			
150	1.561	6.001^2	1.965^3	3.155^3	1.634^3
155	3.740				
160	7.268	9.572^2	3.027^3	4.827^3	2.492^3
165	1.120^1				
170	1.470^1	1.229^3	3.829^3	6.139^3	3.201^3
175					
180	1.795^1	1.331^3	4.128^3	6.643^3	3.479^3
θ^1_{min}	39°	24°	35°	—	77°
θ^2_{min}	148°	125°	120°	117°	121°

In accordance with the present calculation, the general features of the differential cross section show:

(i) a sharp forward peak;

(ii) a peak in the backward direction;

(iii) the formation of double minima at energies below 70 eV;

(iv) a third minima slowly taking shape above 70 eV.

Table 7. (continued)

	E(eV)				
θ(deg)	20	30	40	50	60
0	2.889^{4}	3.674^{4}	4.166^{4}	4.364^{4}	4.355^{4}
5	2.375^{4}	2.839^{4}	3.080^{4}	3.104^{4}	2.976^{4}
10	1.899^{4}	2.084^{4}	2.123^{4}	2.019^{4}	1.836^{4}
15					
20	1.217^{4}	1.065^{4}	8.841^{3}	7.241^{3}	5.870^{3}
25					
30	7.578^{3}	5.092^{3}	3.192^{3}	2.177^{3}	1.609^{3}
35					
40	4.133^{3}	2.109^{3}	8.998^{2}	4.244^{2}	2.489^{2}
45				1.328^{2}	5.379^{1}
50	1.821^{3}	6.925^{2}	1.763^{2}	3.300^{1}	1.637^{1}
55			7.312^{1}	3.852^{1}	6.126^{1}
60	5.468^{2}	1.341^{2}	5.100^{1}	9.342^{1}	1.381^{2}
65	2.397^{2}	5.342^{1}	7.286^{1}		
70	1.106^{2}	5.244^{1}	1.121^{2}	2.071^{2}	2.598^{2}
75	1.134^{2}	1.009^{2}		2.315^{2}	
80	1.983^{2}	1.790^{2}	1.913^{2}	2.333^{2}	2.553^{2}
85	3.167^{2}	2.695^{2}			
90	4.353^{2}	3.537^{2}	2.521^{2}	1.903^{2}	1.615^{2}
95	5.269^{2}				
100	5.747^{2}	4.541^{2}	2.742^{2}	1.284^{2}	6.387^{1}
105	5.723^{2}	4.634^{2}			3.163^{1}
110	5.253^{2}	4.427^{2}	2.522^{2}	8.152^{1}	1.240^{1}
115	4.500^{2}				3.352
120	3.681^{2}	3.160^{2}	1.720^{2}	4.140^{1}	4.840^{-1}
125	3.027^{2}			2.347^{1}	7.406^{-1}
130	2.740^{2}	1.530^{2}	7.296^{1}	1.027^{1}	2.753
135	2.976^{2}	8.981^{1}	3.384^{1}	4.138	7.592
140	3.821^{2}	4.868^{1}	8.586	7.969	1.854^{1}
145	5.266^{2}	3.576^{1}	3.520	2.543^{1}	
150	7.198^{2}	5.407^{1}	2.102^{1}	5.882^{1}	7.271^{1}
155		9.917^{1}	5.584^{1}	1.065^{2}	
160	1.174^{3}	1.604^{2}	9.991^{1}	1.623^{2}	1.677^{2}
165					
170	1.572^{3}	2.873^{2}	1.971^{2}	2.603^{2}	2.691^{2}
175					
180	1.737^{3}	3.471^{2}	2.517^{2}	2.960^{2}	3.163^{2}
$\theta^{1}_{\min}$	72°	67°	59°	52°	49°
$\theta^{2}_{\min}$	130°	145°	144°	136°	122°
σ_{MT}	8.177	4.078	2.473	1.707	1.430

The sharp forward peak arises mainly from high partial waves and becomes more pronounced as the incident energy increases. As the ground-state dipole static polarisability of Kr is larger than that of He, Ne and Ar, more higher partial waves contribute to the cross section and hence the forward peak becomes sharper. Confirmation of the present calculations for small angle scattering from krypton comes from recent unpublished experimental measurements of Wagenaar (1984).

The peak in the backward direction reflects the difficulty of penetration by the incident electron. As the target atom becomes heavier, the probability of the incident

Table 7. (continued)

	E(eV)				
θ(deg)	70	80	90	100	120
0	4.380^{4}	4.274^{4}	4.085^{4}	4.002^{4}	4.081^{4}
5	2.895^{4}	2.730^{4}	2.527^{4}	2.419^{4}	2.312^{4}
10	1.702^{4}	1.536^{4}	1.366^{4}	1.268^{4}	1.125^{4}
15	9.339^{3}	8.128^{3}	7.027^{3}	6.419^{3}	5.628^{3}
20	5.047^{3}	4.293^{3}	3.640^{3}	3.290^{3}	2.857^{3}
25	2.661^{3}	2.203^{3}	1.822^{3}	1.592^{3}	1.342^{3}
30	1.278^{3}	1.015^{3}	8.151^{2}	6.748^{2}	3.199^{2}
35	5.115^{2}	3.741^{2}	2.825^{2}	2.139^{2}	1.629^{2}
40	1.436^{2}	8.436^{1}	5.860^{1}	4.314^{1}	7.255^{1}
45	1.892^{1}	1.431^{1}	2.710^{1}	5.058^{1}	1.239^{2}
50	3.583^{1}	6.528^{1}	9.581^{1}	1.403^{2}	2.299^{2}
55	1.199^{2}	1.682^{2}	2.015^{2}	2.476^{2}	3.251^{2}
60	2.185^{2}	2.706^{2}	2.948^{2}	3.260^{2}	3.687^{2}
65	2.953^{2}	3.361^{2}	3.493^{2}	3.580^{2}	3.545^{2}
70	3.289^{2}	3.527^{2}	3.497^{2}	3.339^{2}	2.886^{2}
75	3.175^{2}	3.207^{2}	3.003^{2}	2.644^{2}	1.971^{2}
80	2.704^{2}	2.525^{2}	2.223^{2}	1.765^{2}	1.033^{2}
85	2.008^{2}	1.706^{2}	1.360^{2}	9.193^{1}	3.390^{1}
90	1.273^{2}	9.443^{1}	6.458^{1}	3.449^{1}	4.406
95	6.543^{1}	3.964^{1}	2.465^{1}	1.772^{1}	1.986^{1}
100	2.376^{1}	1.450^{1}	2.122^{1}	4.117^{1}	7.278^{1}
105	4.831	1.716^{1}	4.920^{1}	9.345^{1}	1.475^{2}
110	4.632	3.907^{1}	9.491^{1}	1.564^{2}	2.231^{2}
115	1.557^{1}	6.697^{1}	1.414^{2}	2.121^{2}	2.771^{2}
120	2.886^{1}	8.872^{1}	1.714^{2}	2.409^{2}	2.935^{2}
125	3.671^{1}	9.636^{1}	1.747^{2}	2.328^{2}	2.692^{2}
130	3.775^{1}	8.710^{1}	1.498^{2}	1.899^{2}	2.096^{2}
135	3.507^{1}	6.680^{1}	1.053^{2}	1.251^{2}	1.322^{2}
140	3.336^{1}	4.596^{1}	5.891^{1}	6.090^{1}	5.723^{1}
145	4.117^{1}	3.564^{1}	2.759^{1}	1.710^{1}	8.860
150	6.545^{1}	4.512^{1}	2.539^{1}	8.810	4.128
155	1.062^{2}	7.808^{1}	5.814^{1}	4.246^{1}	4.917^{1}
160	1.605^{2}	1.323^{2}	1.223^{2}	1.146^{2}	1.361^{2}
165	2.216^{2}	1.969^{2}	2.054^{2}	2.088^{2}	2.452^{2}
170	2.774^{2}	2.570^{2}	2.847^{2}	2.965^{2}	3.533^{2}
175	3.160^{2}	3.019^{2}	3.421^{2}	3.593^{2}	4.352^{2}
180	3.298^{2}	3.197^{2}	3.642^{2}	3.839^{2}	4.635^{2}
$\theta^{1}_{\min}$	47°	45°	44°	42°	40°
$\theta^{2}_{\min}$	107°	102°	98°	94°	91°
$\theta^{3}_{\min}$	139°	145°	148°	149°	148°
σ_{MT}	1.469	1.571	1.782	1.952	2.116

electron being reflected also increases. The multiple-dip structure of the differential cross section is entirely due to the dominance of a particular partial wave. The D wave dominates the scattering for impact energies below 60 eV. At very low energies, the D-wave dominance is challenged by the close range interactions arising from the S and P waves. Hence the double-dip structure is not well established. At energies above 70 eV, the F wave takes over from the D wave as the most dominant partial wave which gives rise to the triple-dip structure in the differential cross section. It

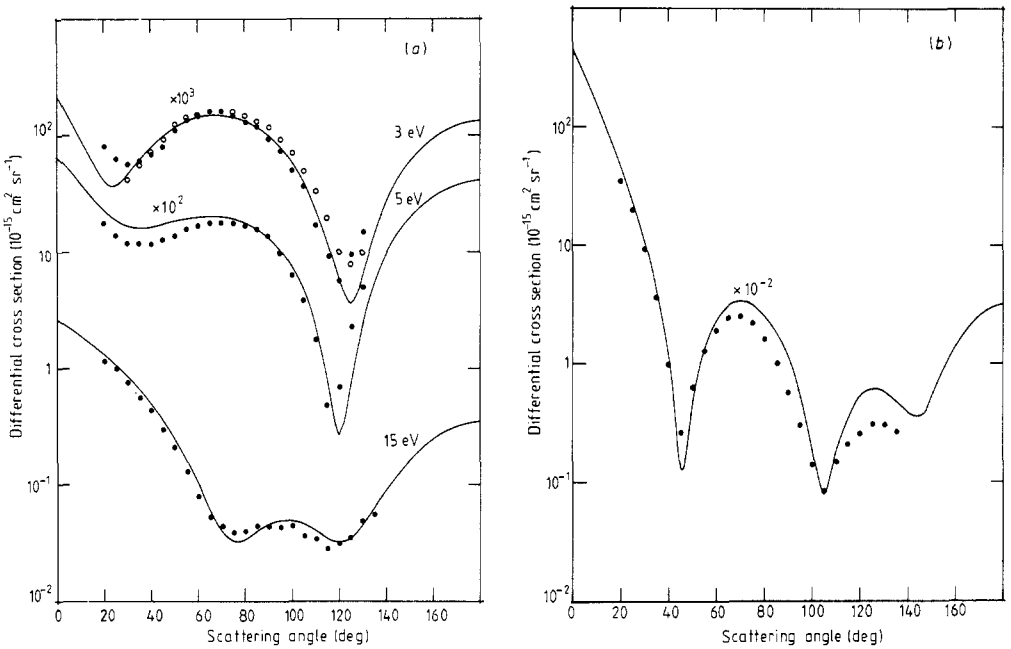

Figure 4. Differential cross section (10^{-15} cm^2 sr^{-1}): (*a*) at 3, 5 and 15 eV, (*b*) at 75 eV. Experiment: ●, Srivastava *et al* (1981); ○, Heindörff *et al* (1976, quoted by Srivastava 1981); Theory: ——, *R* matrix (present).

does seem that the multiple-dip structure arises mainly from the size of the target atom or, in other words, it depends very much on the electron distribution of the target atom. One would not expect this multiple-dip structure to be confined strictly to heavier inert-gas atoms.

At energies below 20 eV there is a striking resemblance between the shapes of the differential cross sections for Kr and those for Ar. Figure 4 shows the present *R*-matrix calculations to be in excellent agreement with the data of Srivastava *et al* (1981) and those of Heindörff *et al* (1976, normalised by Srivastava *et al* 1981).

Figure 5 shows excellent qualitative agreement between the present *R*-matrix calculations and the experiments of Williams and Crowe (1975), Jansen and de Heer (1976) and Srivastava *et al* (1981). The angular positions of the maxima and minima are correctly predicted, although the height and the depth of these maxima and minima are not quite correctly reproduced. The shape of the differential cross sections obtained by McCarthy *et al* (1977) is not quite in accord with those measured by Williams and Crowe (1975). The agreement between the present *R*-matrix calculations and those measured by Srivastava *et al* (1981) is reasonable. The experiments of Srivastava *et al* (1981) tend to lie below the present calculations and the experiments of Williams and Crowe. In making these comparisons, one must bear in mind that over the energy range from 30–100 eV, the cross section curve changes its shape very rapidly with increasing impact energies. It has to change from a developing double-dip structure to make room for a third dip within a narrow energy range of 70 eV. Hence it is more difficult to get the position and magnitude of the cross section correctly at these dips. This not only provides a very stringent test of the theoretical models, but also demands angular and energy resolution of highest precision from the experimentalists. Further theoretical and experimental investigations are needed to show a pattern of consistency.

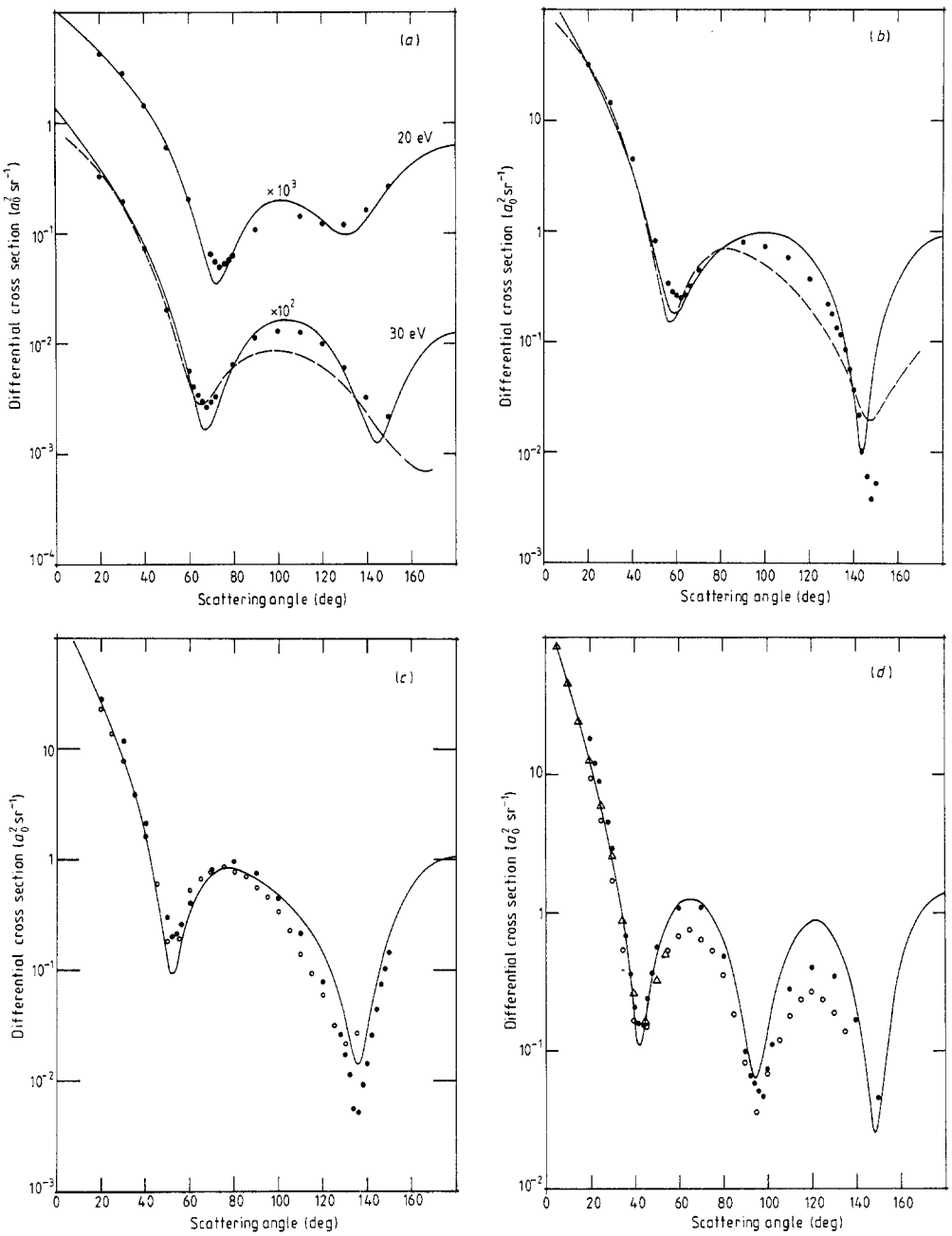

Figure 5. Differential cross section ($a_0^2\,\mathrm{sr}^{-1}$): (*a*) 20 and 30 eV; (*b*) 40 eV; (*c*) 50 eV; (*d*) 100 eV. Experiments: ●, Williams and Crowe (1975); ⊙, Srivastava *et al* (1981). Theory: ——, *R* matrix (present); — —, McCarthy *et al* (1977).

5. Conclusion

It is shown that the *R*-matrix calculations described in I to III, in which the ground-state wavefunction is coupled with a ^{1}P pseudo-state to allow for the ground-state static

dipole polarisability, give for Kr all-round satisfactory agreement with experiments on elastic integral, momentum transfer and differential cross sections. It is also shown that the need for a highly accurate determination of static dipole polarisability may not be so important as it is masked by the competing short-range correlations and the effects of higher multipoles. Further work on xenon is in progress.

Acknowledgments

The authors wish to thank Drs D G Thompson and K L Bell for illuminating discussions. One of us (WCF) would like to acknowledge his gratitude to the International Centre for Theoretical Physics at Trieste (Italy) and the Japanese Authority for the award of ICTP Associateship; to Professors P G Burke and A E Kingston for encouragement and assistance; and to the Department of Applied Mathematics, The Queen's University of Belfast, Northern Ireland, for the hospitality during his visit to Belfast. All the computer calculations were carried out on the CRAY-1 at the SERC, Daresbury Laboratory, England, using a computer workstation provided by the SERC.

References

Arnot F L 1931 *Proc. R. Soc.* A **133** 615–36
Berg R A 1982 *J. Phys. B: At. Mol. Phys.* **15** 3769–77
Berg R A, Purcell J E and Green A E S 1971 *Phys. Rev.* A **3** 508–10
Berrington K A, Burke P G, Le Dourneuf M, Robb W C, Taylor K T and Vo Ky Lan 1978 *Comput. Phys. Commun.* **14** 367–412
Bransden B H and McDowell M R C 1978 *Phys. Rep.* **46** 249–394
Bromberg J P 1974 *J. Chem. Phys.* **61** 963–9
Burke P G, Berrington K A and Sukumar C V 1981 *J. Phys. B: At. Mol. Phys.* **14** 289–305
Clementi E and Roetti C 1974 *At. Data* **14** 177–478
Dababneh M S, Kauppila W E, Downing J P, Laperriere F, Pol V, Smart J H and Stein T S 1980 *Phys. Rev.* A **22** 1872–7
Fink M and Yates A 1970 *At. Data* **1** 385–456
Fon W C and Berrington K A 1981 *J. Phys. B: At. Mol. Phys.* **14** 323–34
Fon W C, Berrington K A, Burke P G and Hibbert A 1983 *J. Phys. B: At. Mol. Phys.* **16** 307–21
Fon W C, Berrington K A and Hibbert A 1981 *J. Phys. B: At. Mol. Phys.* **14** 307–21
Frost L S and Phelps A V 1964 *Phys. Rev.* **136** A1538–45
de Heer F J, Jansen R H and van der Kaay W 1979 *J. Phys. B: At. Mol. Phys.* **12** 979–1002
Heindörff T, Hofft J and Dabkiewicz P 1976 *J. Phys. B: At. Mol. Phys.* **9** 89–99
Hibbert A 1975 *Comput. Phys. Commun.* **9** 141–72
Holtsmark J 1930 *Z. Phys.* **66** 49–58
Jansen R H J and de Heer F J 1976 *J. Phys. B: At. Mol. Phys.* **9** 213–26
Jansen R H J, de Heer F J, Luyken H J, Van Wingerden B and Blaauw H J 1976 *J. Phys. B: At. Mol. Phys.* **9** 185–212
Kemper F, Awe B, Rosicky F and Feder R 1983 *J. Phys. B: At. Mol. Phys.* **16** 1819–25
Kieffer L J 1971 *At. Data* **2** 293–391
Landolt-Börnstein 1950 *Zahlenwerte und Funkfiionen* vol I (Berlin: Springer)
Lewis B R, McCarthy P J O, Teubner P J O and Weigold E 1974 *J. Phys. B: At. Mol. Phys.* **7** 2549–56
McCarthy I E, Noble C J, Phillips B A and Turnbull A D 1977 *Phys. Rev.* A **15** 2173–85
Mehr J 1967 *Z. Phys.* **198** 345–50
O'Connell J K and Lane N F 1983 *Phys. Rev.* A **27** 1893–903
Ramsauer C 1923 *Ann. Phys., Lpz* **72** 345–52
Ramsauer C and Kollath R 1929 *Ann. Phys., Lpz* **3** 536
—— 1932 *Ann. Phys., Lpz* **12** 837

Rosenberg L, O'Malley T F and Spruch L 1961 *J. Math. Phys.* **2** 491–8
Schackert K 1968 *Z. Phys.* **213** 316–32
Sin Fai Lam A L 1982 *J. Phys. B: At. Mol. Phys.* **15** 119–42
Srivastava S K, Tanaka H, Chutjian A and Trajmar S 1981 *Phys. Rev.* A **23** 2156–66
Vo Ky Lan, Le Dourneuf M and Burke P G 1976 *J. Phys. B: At. Mol. Phys.* **9** 1065–78
Wagenaar R W 1984 private communication (submitted as a thesis to the University of Amsterdam)
Walker D W 1971 *Adv. Phys.* **20** 257–323
—— 1974 quoted by de Heer *et al* (1979).
Webb G M 1935 *Phys. Rev.* **47** 379–83
Williams J F and Crowe A 1975 *J. Phys. B: At. Mol. Phys.* **8** 2233–48
Yau A W, McEachran R P and Stauffer A D 1980 *J. Phys. B: At. Mol. Phys.* **13** 377–84